

Conjugated Polymers for Microwave Applications: Untethered Sensing Platforms and Multifunctional Devices

Siew Ting Melissa Tan, Alexander Giovannitti, Adam Marks, Maximilian Moser, Tyler J. Quill, Iain McCulloch, Alberto Salleo,* and Giorgio E. Bonacchini*

In the past two decades, organic electronic materials have enabled and accelerated a large and diverse set of technologies, from energy-harvesting devices and electromechanical actuators, to flexible and printed (opto)electronic circuitry. Among organic (semi)conductors, organic mixed ion–electronic conductors (OMIECs) are now at the center of renewed interest in organic electronics, as they are key drivers of recent developments in the fields of bioelectronics, energy storage, and neuromorphic computing. However, due to the relatively slow switching dynamics of organic electronics, their application in microwave technology, until recently, has been overlooked. Nonetheless, other unique properties of OMIECs, such as their substantial electrochemical tunability, charge-modulation range, and processability, make this field of use ripe with opportunities. In this work, the use of a series of solution-processed intrinsic OMIECs is demonstrated to actively tune the properties of metamaterial-inspired microwave devices, including an untethered bioelectrochemical sensing platform that requires no external power, and a tunable resonating structure with independent amplitude- and frequency-modulation. These devices showcase the considerable potential of OMIEC-based metadevices in autonomous bioelectronics and reconfigurable microwave optics.


1. Introduction

Metamaterials are engineered media with unconventional electromagnetic wave interaction properties, not achievable

S. T. M. Tan, A. Giovannitti, T. J. Quill, A. Salleo, G. E. Bonacchini
Department of Materials Science and Engineering
Stanford University
Stanford, CA 94305, USA
E-mail: asalleo@stanford.edu; giorgio.bonacchini@iit.it

A. Marks, M. Moser, I. McCulloch
Department of Chemistry
Chemistry Research Laboratory
University of Oxford
Oxford OX1 3TA, UK

G. E. Bonacchini
Center for Nano Science and Technology@PoliMi
Istituto Italiano di Tecnologia
Milan 20133, Italy

 The ORCID identification number(s) for the author(s) of this article can be found under <https://doi.org/10.1002/adma.202202994>.

© 2022 The Authors. Advanced Materials published by Wiley-VCH GmbH. This is an open access article under the terms of the Creative Commons Attribution License, which permits use, distribution and reproduction in any medium, provided the original work is properly cited.

DOI: 10.1002/adma.202202994

by “natural” materials.^[1] Electrically tunable metamaterials, otherwise known as metadevices, are expected to play a transformative role in radar/telecommunication platforms across the microwave and THz spectra (e.g., Internet of Things and 5G),^[2] as well as in transformation optics,^[3] cloaking,^[4] healthcare,^[5] and analogue computing.^[6] A plethora of tuning strategies has been so far proposed for the realization of microwave metadevices. Among electrical strategies, a traditional approach relies on the integration of microwave resonators—the building blocks of metamaterials—with lumped electronic components (e.g., varactor and pin diodes), whereas recent research has increasingly focused on the use of electroactive materials, such as graphene and III–V compound semiconductors.^[7] In both these cases, metadvice tunability is achieved by electrically modulating the population of free charge carriers in the material, thus controlling its complex permittivity through changes in the conductivity.^[3] These tuning strategies however come with high fabrication complexity and cost compared to emerging semiconductor technologies, such as organic electronics, which is compatible with cost-effective and mass-scalable techniques such as printing and coating.^[7–11] Furthermore, neither of these approaches can be easily translated into large-area and/or mechanically conformable platforms, which could prove essential for facile body, vehicle, or building integration.

Although yet unexplored in microwave applications, organic mixed ionic-electronic conductors (OMIECs) are attracting attention for their unique mixed transport properties, their remarkable performance as biotic/abiotic interfaces, and for their exceptional potential in energy storage and neuromorphic devices.^[12–17] The strong ion–electron coupling in these materials enables charge carrier density variations of several orders of magnitude with subvolt polarizations, through volumetric capacitances ranging from few tens to hundreds of $F\text{ cm}^{-3}$. These capacitance values exceed those achievable with high permittivity dielectrics and electrical double layers in field-effect technologies. Indeed, the superior charge modulation in OMIECs make them ideally suited to electrically tune microwave resonators through free carrier absorption.^[7] Moreover, unlike current electroactive materials used in metadevices,

Although yet unexplored in microwave applications, organic mixed ionic-electronic conductors (OMIECs) are attracting attention for their unique mixed transport properties, their remarkable performance as biotic/abiotic interfaces, and for their exceptional potential in energy storage and neuromorphic devices.^[12–17] The strong ion–electron coupling in these materials enables charge carrier density variations of several orders of magnitude with subvolt polarizations, through volumetric capacitances ranging from few tens to hundreds of $F\text{ cm}^{-3}$. These capacitance values exceed those achievable with high permittivity dielectrics and electrical double layers in field-effect technologies. Indeed, the superior charge modulation in OMIECs make them ideally suited to electrically tune microwave resonators through free carrier absorption.^[7] Moreover, unlike current electroactive materials used in metadevices,

organic semiconductors are compatible with solution-phase deposition and patterning techniques on virtually any planar substrate, including those based on plastic, bioinspired, and ultrathin materials.^[10]

Bonacchini and Omenetto recently proposed a device configuration where organic electrochemical transistors (OECTs)—a family of transistors based on OMIECs—actively tune an assorted set of coplanar sub-5 GHz microwave metasurfaces and metamaterial-inspired structures based on split-ring resonators (SRRs).^[18] SRRs effectively operate as inductor-capacitor oscillating circuits, where OECTs can be used to shunt current to or from the coil's inductance and capacitance, thus altering the resonance characteristics of the circuit.^[19–21] In OECTs, because of the volumetric capacitive charging of the OMIEC, conductance changes across the transistor channel are significantly larger than those achievable with conventional field-effect technologies. (poly(3,4-ethylenedioxythiophene):polystyrene sulfonate) (PEDOT:PSS)—the prototypical OMIEC (see the Experimental Section for full chemical name)—was used as the active material in the OECTs due to its favorable conductivity at microwave frequencies, which has been exploited in conductive coatings for electromagnetic interference shielding.^[22] Despite its wide use and large availability, PEDOT:PSS is however a conjugated polymer:polyelectrolyte blend characterized by poor chemical tunability, which imposes fixed boundaries on its electrochemical operation range. Moreover, the conductive nature of this material implies that PEDOT:PSS-based OECTs are depletion-mode transistors rather than enhancement-mode,^[13] with limited control on device operating voltage, conductance range, and stability.^[23]

In this work, we demonstrate that the same tuning strategy can be implemented by using an emerging family of OMIECs constituted by intrinsic polymer semiconductors with glycolated side chains,^[12] which has not yet been explored in microwave applications. Unlike PEDOT-based OMIECs, these polymers display synthetically tunable electrochemical and structural proper-

ties—such as energy levels, redox-activity, microstructure, and modulus—as well as improved electron and ion transport characteristics. Indeed, the superior chemical tunability of these conjugated polymers with polar side chains allows the realization of enhancement-mode OECTs in either p-type, n-type, or ambipolar configurations.^[24,25] Moreover, OECTs based on intrinsic OMIECs outperform PEDOT:PSS-based devices in terms of charge mobility, subthreshold swing, dynamic range, volumetric capacitance, and electrochemical stability.^[23,24,26,27]

The unique characteristics of intrinsic OMIECs thus enable OECT configurations that target distinct operating modes and operating voltage windows, which can be tailored to specific applications, such as in sensors for microwave healthcare technologies.^[5] In this work, we design a wireless system that transduces weak bioelectrochemical voltages without any external biasing circuits, power supplies, or microwave electronics. Moreover, we show that by simultaneously employing different OMIECs on the same resonating structure, multiple OECTs with different electrical characteristics can be operated jointly, thereby achieving complex multifunctional devices in which the resonance amplitude and frequency are independently controllable. In previous works, such dual tuning has been demonstrated through a combination of varactor diodes and graphene supercapacitors on the same metadvice, with the ensuing integration complexity.^[28,29] We show that a judicious choice of materials allows us to achieve the same functionality using exclusively OECTs, thus highlighting that our approach is promising yet simple.

2. Structure, Materials, and Operation of Tunable Resonators

The structure of the tunable resonators used in this work is illustrated in **Figure 1a,b**, and consists of a double broadside-coupled SRR geometry (DBSRR), whose split region of the top SRR is

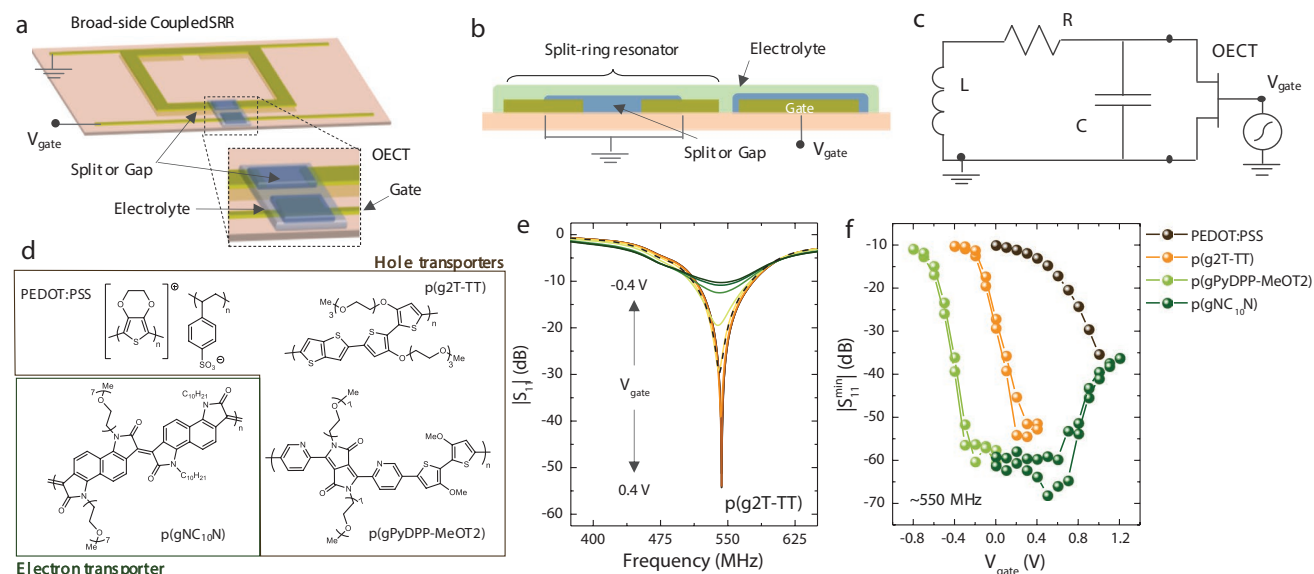


Figure 1. a,b) Illustration of an amplitude-modulated DBSRR a) and its schematic cross-section b). c) Equivalent circuit model of the device, where the OECT is connected in parallel to the capacitive component of the resonator. d) Chemical structures and names of the polymer OMIECs used in this work. e) Amplitude modulation of a p(g2T-TT) based tunable resonator (dashed curved: resonator without OECT). f) Voltage dependence of identical resonators modulated using different polymer OMIECs.

bridged by the OMIEC and gated through an ion-gel electrolyte.^[23] The DBSRR geometry offers a smaller form factor and lower resonance frequency compared to other SRR-based structures with equivalent lateral dimensions^[30–32]—see Figure S2 (Supporting Information) for detailed geometry. In this configuration, the SRR/OECT assembly can be modeled as an inductive-capacitive oscillator where the OECT is placed in parallel to the equivalent capacitance of the split region (Figure 1c). Upon coupling the SRR to an external electromagnetic stimulus, the channel of the transistor acts as a gate-controlled variable resistor, along which the charge carriers are subject to a high-frequency lateral field. When V_{gate} biases the transistor in the ON state, the high charge carrier density in the channel electrically shunts the equivalent capacitor, thereby quenching the resonance.^[18–21]

Besides the conjugated polymer:polyelectrolyte blend of PEDOT:PSS, the three additional OMIEC polymers are characterized by a hole (or electron) transporting backbone with oligo ethylene glycol side chains, which facilitate ionic transport throughout the bulk of the polymer (Figure 1d).^[12] Two of these polymer systems, namely p(g2T-TT) and p(gPyDPP-MeOT2), enable enhancement-mode p-type OECTs. Similarly, the p(gNC₁₀N) polymer was recently proposed in high-performance n-type OECTs. Its backbone is characterized by a planarized structure that favors electron transport along the polymer chains by reducing their conformational disorder.^[33]

Gate potentials within ± 0.4 V on a p(g2T-TT)-channel OECT modulate the amplitude of a DBSRR (Figure 1e). The return losses (S_{11} parameter) measured through a loop antenna adjacent to the device show a variation larger than 40 dB at ≈ 550 MHz, which corresponds to a modulation ratio exceeding four orders of magnitude (see Figure S1, Supporting Information, for equivalent measurements performed on p(gPyDPP-MeOT2) and p(gNC₁₀N)).

A comparison of the behavior of the four different OMIECs is presented in Figure 1f, where the voltage dependence of the devices is illustrated by plotting the minimum of the S_{11} spectra at each gate potential. As expected, while the PEDOT:PSS device exhibits a depletion-mode behavior and moderate modulation, the three conjugated polymers with glycolated side chains operate in enhancement mode, with characteristic driving voltages that are in agreement with equivalent OECT measurements performed with the same materials, and much deeper modulation.^[23,33] Indeed, while tunable DBSRR based on p(g2T-TT) displays the maximum variation in modulation just below 0 V, the pyridine-flanked diketopyrrolopyrrole unit in the p(gPyDPP-MeOT2) determines a significantly lower threshold voltage for the device (≈ -0.4 V), because of the higher ionization energy associated with this chemical structure with respect to the bithiophene–thienothiophene unit of the p(g2T-TT), i.e., 5.0 and 4.5 eV for p(gPyDPP-MeOT2) and p(g2T-TT), respectively.^[23] Note that both these polymers afford a deeper modulation with respect to PEDOT:PSS, in agreement with the larger ON/OFF ratios of OECTs made with these materials.^[26] The electron-transporting polymer p(gNC₁₀N) displays n-type operation ($V_{\text{gate}} > 0$ V) with a threshold voltage set at ≈ 0.6 V, achieving a modulation depth in excess of 20 dB. With respect to the hole-transporting materials investigated in this work, we attribute the comparatively less pronounced modulation of p(gNC₁₀N) to its lower charge mobility—estimated at

$10^{-3} \text{ cm}^2 \text{ V}^{-1} \text{ s}^{-1}$, approximately two orders of magnitude inferior to p(g2T-TT).^[24,33]

3. Wireless and Battery-Less Bioelectrochemical Sensing Platform

The unique voltage characteristics of the tunable resonators described in Figure 1f can be selectively leveraged to target specific functionalities that benefit from the wireless detection of low-voltage signals, for example in bioelectronic and health-care application scenarios. These tunable devices can indeed be exploited to transduce bioelectrochemical signals, while simultaneously encoding the resulting information within the backscattered radiation from the resonators. This combined transduction/modulation scheme is of particular technological appeal when implemented in the so-called S microwave band—2–4 GHz, as designated by the Institute of Electrical and Electronics Engineers (IEEE)—which is largely exploited for a plethora of communication protocols (e.g., Bluetooth, WiFi, medical devices, remote switches, etc.).^[34] This approach eliminates the need for embedded complex and energy-demanding radio-frequency electronics, such as oscillators and modulators, which cannot yet be made at microwave frequencies using organic electronics.^[35] Furthermore, by chemically engineering the OMIEC to achieve low operation voltages, as in the case of p(g2T-TT), the transduction of low amplitude biosignals—usually in range of few tens or hundreds of mV—can occur in the absence of external biasing/amplifying circuits, nor power supplies.

To demonstrate the wireless and battery-less transduction of metabolites in aqueous analytes, a tunable SRR operating at ≈ 2.1 GHz is integrated with a two-electrode enzymatic reaction cell (RC) based on OMIEC electrodes, recently proposed by Tan et al.^[36] The spontaneous faradaic reactions on the RC modulates the microwave response of the tunable SRR, effectively powering the changes in OECT channel conductance, and thus making the device fully autonomous and untethered. By designing the tunable SRR with an ion-gel electrolyte and decoupling the microwave transducer from the aqueous electrolyte hosting the enzymatic reaction, we avoid undesired interactions between the biological sensing medium and the tuning element in the SRR. As OECT channel material, we chose p(g2T-TT) for its operating voltage window, which displays a maximum variation in modulation close to 0 V. This polymer is thus suitable for transducing the voltages generated by the RC, which amount to few hundreds of mV. We hence fabricated a p(g2T-TT)-channel tunable SRR operating at ≈ 2.1 GHz, which was electrically coupled to the coplanar RC (Figure 2a) loaded with glucose oxidase (GOx).^[36] When exposed to glucose in physiological solution (phosphate buffer solution, PBS), the enzyme-catalyzed faradaic reaction (Figure 2b) converts glucose and forms hydrogen peroxide, which then oxidizes the OMIEC anode. This process establishes an electrical potential $V_{\text{RC}} = V^+ - V^-$ across the anode and cathode terminals, which is then transduced by the OECT. The conductance change in the OECT is wirelessly recorded by monitoring the resonance amplitude of the resonator versus time.^[36] Figure 2c displays the microwave spectra before and after the reaction cell was exposed to glucose, while Figure 2d reports the time variations

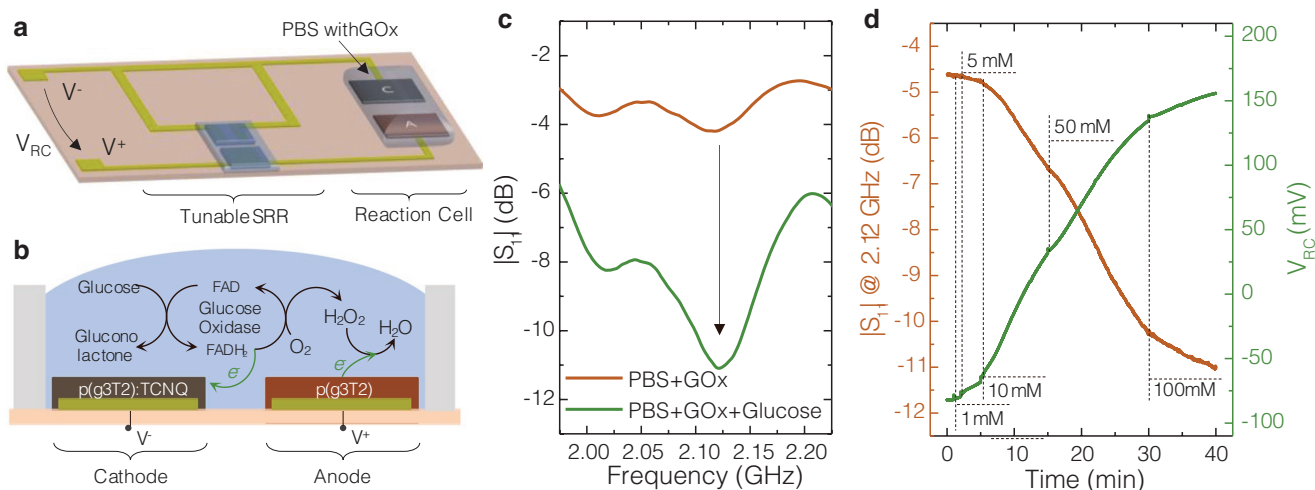


Figure 2. a) Scheme of the SRR/RC assembly. b) Representation of the enzymatic redox reaction taking place within the electrochemical cells, and of the electron transfer reactions occurring at the anodic and cathodic electrodes based on the conjugated polymer OMIEC p(g3T2) and p(g3T2) doped with TCNQ, respectively. c) S_{11} spectra of the tunable SRR/reaction cell assembly connected in the gate-to-anode configuration, before and after glucose was added to the electrolyte. d) Time-dependent variation of the resonance amplitude upon glucose administration (brown) and of the electrochemical potential V_{RC} gating the tunable resonator (green).

of both the electrochemical potential V_{RC} and the S_{11} parameter at resonance upon glucose introduction. In the absence of glucose, the negative electrochemical equilibrium potential with the initial PBS and GOx solution charges the OECT channel, thus quenching the resonance, but V_{RC} gradually increases as aliquots of glucose solution are added to the enzymatic cell, hence turning OFF the OECT. As expected, this change in V_{RC} from ≈ -80 to about 150 mV is accompanied by an increase in the resonance depth (from -4.5 to -11 dB), with the resonator dynamics closely following those of the reaction cell (see Figure S3, Supporting Information, for time-dependent pulsed measurement performed on the tunable SRR).

4. Independent Amplitude and Frequency Control

With this family of OMIECs, chemical design can be exploited to achieve other unique functionalities in microwave devices, such as a reconfigurable microwave structure that is either amplitude or frequency tunable depending on the applied gate voltage. This is achieved by embedding multiple OECTs based on different polymers on the same individual resonator, deliberately exploiting the distinct operating voltages characteristic of the individual OMIECs. This dual mode of operation could for example prove useful in cloaking applications, where one would want to tune the frequency response and also turn the cloak on and off. It is however still elusive and it has not yet been demonstrated in a metadvice using exclusively one tuning strategy and a single device type.^[28,29]

Figure 3a displays the schematics of an amplitude and frequency tunable DBSRR, whose top SRR features a pair of splits with different lateral widths. Both these splits contribute capacitively to the equivalent circuit model— C_L and C_R , respectively, in Figure 3b—and each is connected in parallel to a different p-type OECT sharing the same gate electrode potential V_{gate} . In particular, the widest split (L) is bridged by a PEDOT:PSS

channel, which is highly conductive at $V_{gate} \leq 0$ V, while the narrowest one (R) features a p(gPyDPP-MeOT2) channel, which exhibits a high conductivity state only below the threshold voltage of -0.4 V—the lowest threshold voltage among the OMIECs explored in this study. For this reason, at $V_{gate} = 0$ V this structure displays a resonant behavior, with a resonance frequency $f_0 = 1/(2\pi\sqrt{LC_R})$ determined exclusively by the capacitive contribution of the R split. The resonance can hence be quenched according to the mechanism previously described in Figure 1: as the gate potential is gradually decreased below 0 V, the p(gPyDPP-MeOT2) channel is electrostatically doped, thus shunting C_R , while the PEDOT:PSS channel remains highly conductive.

Conversely, the frequency of the resonator can be modulated by alternating between the contribution of only one split—, i.e., C_R in this case—and the series connection between C_L and C_R , which amounts to a cumulative capacitive contribution equal to $C_{series} = C_L C_R / (C_R + C_L)$. Since $C_R > C_{series}$, the resulting frequency is shifted toward higher values when both capacitors are contributing in series. This mode of operation is achieved by driving the common gate potential toward positive values, thus dedoping the PEDOT:PSS channel, while the p(gPyDPP-MeOT2) remains in the low conductivity state.

Figure 3c,d reports the voltage-dependence of this device configuration. Note that the frequency modulation is evidently associated to a variation in amplitude, particularly at voltage levels where the depletion-mode OECT is not entirely OFF. This behavior is likely due to the low, yet non-negligible conductivity of the PEDOT:PSS channel at intermediate voltages, and it is common to other well-established frequency-modulation strategies.^[4,37]

5. Conclusion

This work explores the use of a novel class of conjugated polymer semiconductors as tuning elements within microwave

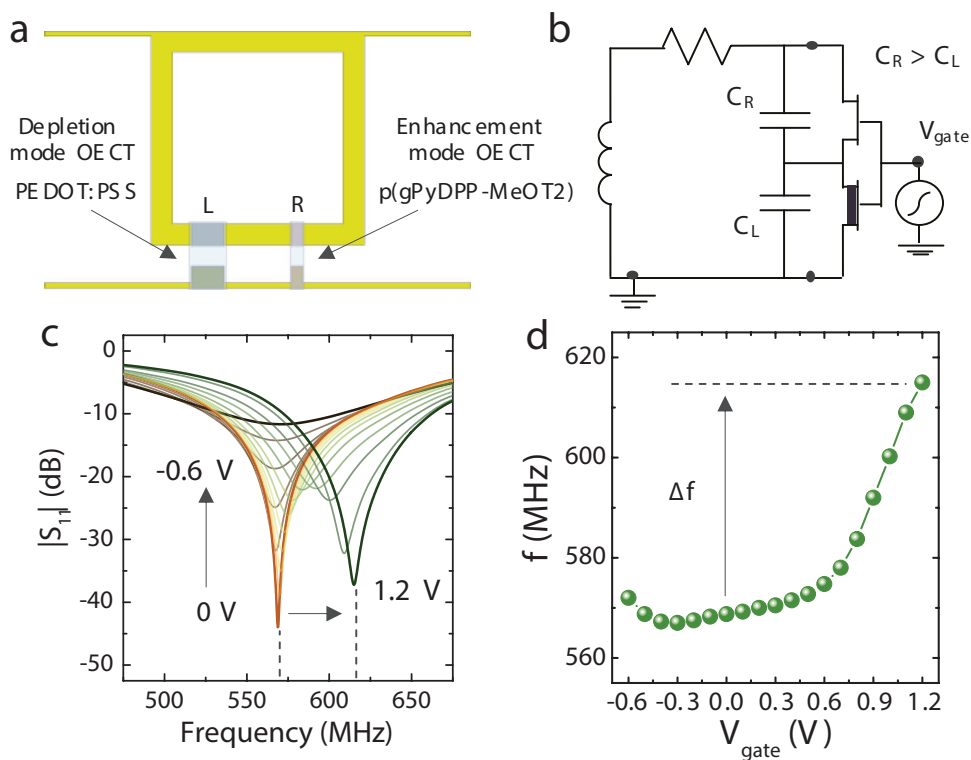


Figure 3. a) Schematic of a tunable DBSRR with independently controllable amplitude and frequency. b) Equivalent electrical circuit model of the device, where the depletion-mode transistor is placed in parallel to C_L , while the enhancement-mode OE CT is in parallel to C_R , and both are gated with the same V_{gate} potential. c) S_{11} spectra demonstrating amplitude and frequency tuning by applying negative and positive gate potentials, respectively. d) Voltage-dependence of the resonance frequency.

SRRs, which constitute the building blocks of emerging metadevice technologies. The unique redox-tunability and charge modulation capability of these electroactive materials, traditionally considered unsuitable to radio-frequency and microwave applications, pave the way for a generation of microwave devices with bespoke operating modes and conditions, while maintaining performances comparable to other state-of-the-art metadevice tuning strategies.^[18] Nonetheless, much is yet to be understood about the properties of OMIECs operating in microwave structures, at both the materials and the device level. For example, the spectral limitations of this tuning strategy are fundamentally unknown, as the traditional structure-function relationships of this class of semiconductors are not well studied at the radio-frequencies of interest here. Future investigations will address these fundamental questions, while also exploring new metadevice configurations and applications based on this tuning strategy. The proof-of-concept devices described in this work indeed suggest that OMIEC-based reconfigurability could potentially lead to new and unexplored photonic platforms across the microwave spectrum, and possibly all the way to the THz.^[38,39] Examples of such applications include untethered and self-powered neural interfaces able to transduce signals from electrogenic cells and tissues, implantable/wearable, and self-powered microwave systems for healthcare applications, and multifunctional reconfigurable metasurfaces fabricated on large areas with cost-effective techniques and environmentally sustainable materials.

6. Experimental Section

Materials: Polyimide substrates ($\approx 50 \mu\text{m}$ thick) were purchased from Sigma-Aldrich, and used without cleaning. Ionic liquid 1-ethyl-3-methylimidazolium bis(trifluoromethylsulfonyl)imide (EMIM:TFSI) was purchased from Iolitec (99.5% grade, respectively). Polymeric insulator poly(vinylidene fluoride-co-hexafluoropropylene) (PVDF-HFP) pellets with an average M_w (weight-average molecular weight) of ≈ 400000 and an average M_n (number-average molecular weight) of ≈ 130000 were purchased from Sigma-Aldrich. The PEDOT:PSS was purchased from Heraeus (Clevios P Jet 700 printable ink). The polymers p(g2T-TT) (poly(2-(3,3'-bis(2-(2-(2-methoxyethoxy)ethoxy)ethoxy)-[2,2-bithiophen]-5-yl)thieno[3,2-b]thiophene)), p(gPyDPP-MeOT2) (poly(3-(5-(3,3''-dimethoxy-5''-methyl-[2,2''-bithiophen]-5-yl)pyridin-2-yl)-2,5-di(2,5,8,11,14,17,20-heptaaxadocosan-22-yl)-6-(5-methylpyridin-2-yl)-2,5-dihydropyrrolo[3,4-c]pyrrole-1,4-dione)), and p(gNC₁₀N) (poly((E)-3,8-didecyl-3'',8''-di(2,5,8,11,14,17,20-heptaaxadocosan-22-yl)-6,6''-dimethylene-6,6'',8,8'-tetrahydro-2H,2'H-[1,1'-biindolo[7,6-g]indolylidene]-2,2',7,7'-(3H,3'H)-tetraone)) were synthesized according to the methods discussed.^[23,24,33] p(g3T2) (3,3'-dialkoxybithiophene) was synthesized according to ref. [40]. Tetracyanoquinodimethane (TCNQ) was purchased from Sigma-Aldrich.

Tunable SRR Fabrication: The metal patterns of tunable resonators were deposited by means of thermal evaporation (Cr/Au: 5 nm/100 nm) through a shadow mask. The OMIECs were either spin-coated (PEDOT:PSS, 1000 rpm for 60 s, followed by annealing at 120 °C for 30 min) or drop-cast directly on the channel and gate of the devices (≈ 10 and 20 μL respectively, to ensure larger capacitance at the gate with respect to the channel). In PEDOT:PSS and p(g2T-TT) devices, the gate electrode was coated with the same material used for the channel, whereas TCNQ-doped p(g3T2) was used as gating material in the p(gPyDPP-MeOT2) and

p(gNC₁₀N) devices. Ion gels were prepared according to ref. [26] and drop-cast on the transistor channel and gate area ($\approx 10 \mu\text{L}$ per device).

Reaction Cell Fabrication: Polymer electrodes were drop-cast on evaporated gold electrodes on the same polyimide substrate as the tuneable SRR. The anode consists of p(g3T2), while the cathode consists of 60 mol% TCNQ-doped p(g3T2). A PDMS well was placed around the electrodes to confine the aqueous analyte.

Electrochemical Measurements: 100 μL 20.4 mg mL⁻¹ of Glucose Oxidase Type II in PBS was deposited in the RC well and 10 μL of glucose dissolved in PBS of various concentrations were added to the well at different time intervals. The potential change across the RC was measured in a two-electrode setup using an Ivium Potentiostat.

Microwave Characterization: The scattering parameters were acquired using a primary coil connected to a Vector Network Analyzer (Rohde&Schwartz ZNB4.22). Devices were biased using a source-measure unit (Keithley 2600).

Supporting Information

Supporting Information is available from the Wiley Online Library or from the author.

Acknowledgements

The authors thank the Stanford Prototyping Facility, where the microwave measurements took place, and John Ho (National University of Singapore) for the useful discussions. G.E.B. gratefully acknowledges support from the European Union's Horizon 2020 research and innovation programme under the Marie Skłodowska-Curie Grant Agreement No. 838799 – LEAPh.

Open access funding provided by Istituto Italiano di Tecnologia within the CRUI-CARE Agreement.

Conflict of Interest

The tuning strategy presented in this Article is the object of a U.S. Patent Application (No. 17/449935) filed by Tufts University, with Giorgio E. Bonacchini and Fiorenzo G. Omenetto as inventors.

Data Availability Statement

The data that support the findings of this study are openly available in Zenodo at <https://doi.org/10.5281/zenodo.6719789>.

Keywords

microwave devices, organic mixed conductors, wireless sensing

Received: April 1, 2022

Revised: June 6, 2022

Published online: July 15, 2022

[1] J. B. Pendry, D. Schurig, D. R. Smith, *Science* **2006**, *312*, 1780.

[2] O. Quevedo-Teruel, H. Chen, A. Díaz-Rubio, G. Gok, A. Grbic, G. Minatti, E. Martini, S. Maci, G. V. Eleftheriades, M. Chen, N. I. Zheludev, N. Papisimakis, S. Choudhury, Z. A. Kudyshev, S. Saha, H. Reddy, A. Boltasseva, V. M. Shalaev, A. V. Kildishev,

D. Sievenpiper, C. Caloz, A. Al, Q. He, L. Zhou, G. Valerio, E. Rajo-Iglesias, Z. Sipus, F. Mesa, R. Rodríguez-Berral, F. Medina, et al., *J. Opt.* **2019**, *21*, 073002.

[3] N. I. Zheludev, Y. S. Kivshar, *Nat. Mater.* **2012**, *11*, 917.

[4] C. Qian, B. Zheng, Y. Shen, L. Jing, E. Li, L. Shen, H. Chen, *Nat. Photonics* **2020**, *14*, 383.

[5] Z. Li, X. Tian, C.-W. Qiu, J. S. Ho, *Nat. Electron.* **2021**, *4*, 382.

[6] F. Zangeneh-Nejad, D. L. Sounas, A. Alù, R. Fleury, *Nat. Rev. Mater.* **2020**, *6*, 207.

[7] Q. He, S. Sun, L. Zhou, *Research* **2019**, *2019*, 1849272.

[8] X. Zhao, G. Duan, A. Li, C. Chen, X. Zhang, *Microsyst. Nanoeng.* **2019**, *5*, 5.

[9] A. Nemat, Q. Wang, M. Hong, J. Teng, *Opto-Electron. Adv.* **2018**, *1*, 18000901.

[10] M. Caironi, Y.-Y. Noh, *Large Area and Flexible Electronics*, Wiley-VCH, Weinheim, Germany **2015**.

[11] X. Guo, A. Facchetti, *Nat. Mater.* **2020**, *19*, 922.

[12] B. D. Paulsen, K. Tybrandt, E. Stavrinidou, J. Rivnay, *Nat. Mater.* **2020**, *19*, 13.

[13] J. Rivnay, S. Inal, A. Salleo, R. M. Owens, M. Berggren, G. G. Malliaras, *Nat. Rev. Mater.* **2018**, *3*, 17086.

[14] S. Ting, M. Tan, A. Gumyusenge, T. J. Quill, G. Swain Lecroy, G. E. Bonacchini, I. Denti, A. Salleo, S. T. M. Tan, A. Gumyusenge, T. J. Quill, G. S. Lecroy, G. E. Bonacchini, I. Denti, A. Salleo, *Adv. Mater.* **2022**, *34*, 2110406.

[15] D. Ohayon, S. Inal, *Adv. Mater.* **2020**, *32*, 2001439.

[16] Y. Van De Burgt, A. Melianas, S. T. Keene, G. Malliaras, A. Salleo, *Nat. Electron.* **2018**, *1*, 386.

[17] F. Jiao, J. Edberg, D. Zhao, S. Puzinas, Z. Ullah Khan, P. Mäkie, A. Naderi, T. Lindström, M. Odén, I. Engquist, M. Berggren, X. Crispin, S. F. Jiao, J. Edberg, D. Zhao, S. Puzinas, Z. U. Khan, I. Engquist, M. Berggren, X. Crispin, P. Mäkie, M. Odén, *Adv. Sustainable Syst.* **2018**, *2*, 1700121.

[18] G. E. Bonacchini, F. G. Omenetto, *Nat. Electron.* **2021**, *4*, 424.

[19] H. T. Chen, W. J. Padilla, J. M. O. Zide, A. C. Gossard, A. J. Taylor, R. D. Averitt, *Nature* **2006**, *444*, 597.

[20] S. Venkatesh, X. Lu, H. Saeidi, K. Sengupta, *Nat. Electron.* **2020**, *3*, 785.

[21] A. Hai, V. C. Spanoudaki, B. B. Bartelle, A. Jasanoff, *Nat. Biomed. Eng.* **2019**, *3*, 69.

[22] Y. Wu, Z. Wang, X. Liu, X. Shen, Q. Zheng, Q. Xue, J. K. Kim, *ACS Appl. Mater. Interfaces* **2017**, *9*, 9059.

[23] A. Giovannitti, R. B. Rashid, Q. Thiburce, B. D. Paulsen, C. Cendra, K. Thorley, D. Moia, J. T. Mefford, D. Hanifi, D. Weiyuan, M. Moser, A. Salleo, J. Nelson, I. McCulloch, J. Rivnay, *Adv. Mater.* **2020**, *32*, 1908047.

[24] A. Giovannitti, D.-T. Sbircea, S. Inal, C. B. Nielsen, E. Bandiello, D. A. Hanifi, M. Sessolo, G. G. Malliaras, I. McCulloch, J. Rivnay, *Proc. Natl. Acad. Sci. USA* **2016**, *113*, 12017.

[25] A. Giovannitti, C. B. Nielsen, D.-T. Sbircea, S. Inal, M. Donahue, M. R. Niazi, D. A. Hanifi, A. Amassian, G. G. Malliaras, J. Rivnay, I. McCulloch, *Nat. Commun.* **2016**, *7*, 13066.

[26] A. Melianas, T. J. Quill, G. LeCroy, Y. Tuchman, H. V. Loo, S. T. Keene, A. Giovannitti, H. R. Lee, I. P. Maria, I. McCulloch, A. Salleo, *Sci. Adv.* **2020**, *6*, eabb2958.

[27] V. Venkatraman, J. T. Friedlein, A. Giovannitti, I. P. Maria, I. McCulloch, R. R. McLeod, J. Rivnay, *Adv. Sci.* **2018**, *5*, 1800453.

[28] J. Zhang, X. Wei, I. D. Rukhlenko, H. T. Chen, W. Zhu, *ACS Photonics* **2020**, *7*, 265.

[29] C. Huang, C. Ji, B. Zhao, J. Peng, L. Yuan, X. Luo, *Adv. Mater. Technol.* **2021**, *6*, 2001050.

[30] R. Marqués, F. Mesa, J. Martel, F. Medina, *IEEE Trans. Antennas Propag.* **2003**, *51*, 2572.

[31] J. Wang, S. Qu, J. Zhang, H. Ma, Y. Yang, C. Gu, X. Wu, Z. Xu, *Prog. Electromagn. Res. Lett.* **2009**, *6*, 35.

- [32] P. Tseng, B. Napier, L. Garbarini, D. L. Kaplan, F. G. Omenetto, *Adv. Mater.* **2018**, *30*, 1703257.
- [33] X. Chen, A. Marks, B. D. Paulsen, R. Wu, R. B. Rashid, H. Chen, M. Alsufyani, J. Rivnay, I. McCulloch, *Angew. Chem., Int. Ed.* **2021**, *60*, 9368.
- [34] *IEEE Standard for Radar Definitions*, in IEEE 686-2017 (Revision of IEEE Std 686-2008), IEEE, Piscataway, NJ, USA **2017**, pp. 1–54.
- [35] U. Zschieschang, J. W. Borchert, M. Giorgio, M. Caironi, F. Letzkus, J. N. Burghartz, U. Waizmann, J. Weis, S. Ludwigs, H. Klauk, *Adv. Funct. Mater.* **2020**, *30*, 1903812.
- [36] S. T. M. Tan, A. Giovannitti, A. Melianas, M. Moser, B. L. Cotts, D. Singh, I. McCulloch, A. Salleo, *Adv. Funct. Mater.* **2021**, *31*, 2010868.
- [37] O. Balci, N. Kakenov, E. Karademir, S. Balci, S. Cakmakyapan, E. O. Polat, H. Caglayan, E. Ozbay, C. Kocabas, *Sci. Adv.* **2018**, *4*, eaao1749.
- [38] Y. Du, X. Cui, L. Li, H. Tian, W.-X. Yu, Z.-X. Zhou, *Phys. Status Solidi* **2018**, *255*, 1700547.
- [39] F. Yan, E. P. J. Parrott, B. S. Y. Ung, E. Pickwell-Macpherson, *J. Phys. Chem. C* **2015**, *119*, 6813.
- [40] D. Moia, A. Giovannitti, A. A. Szumska, I. P. Maria, E. Rezasoltani, M. Sachs, M. Schnurr, P. R. F. Barnes, I. McCulloch, J. Nelson, *Energy Environ. Sci.* **2019**, *12*, 1349.